A New Type of Quartz Smog Chamber : Design and Characterization

Ma, Wei

2022-02-15

Ma , W , Liu , Y , Zhang , Y , Feng , Z , Zhan , J , Hua , C , Ma , L , Guo , Y , Zhang , Y , Zhou , W , Yan , C , Chu , B , Chen , T , Ma , Q , Liu , C , Kulmala , M , Mu , Y & He , H 2022 , ' A New Type of Quartz Smog Chamber : Design and Characterization ' , Environmental þÿ S c i e n c e a n d T e c h n o l o g y , v o l . 5 6 , n o . 4 , p p . 2 1 8 1 2 1 9 0 . h t t p s : / / d o i .

http://hdl.handle.net/10138/341590
https://doi.org/10.1021/acs.est.1c06341

unspecified

A New Type of Quartz Smog Chamber: Design and Characterization

Wei Ma[1], Yongchun Liu[1,5*], Yusheng zhang[1], Zemin Feng[1], Junlei Zhan[1], Chenjie Hua[1], Li Ma[1], Yishuo Guo[1], Ying Zhang[1], Wenshuo Zhou[1], Chao Yan[2], Biwu Chu[3], Tianzeng Chen[3], Qingxin Ma[3], Chunshan Liu[4], Markku Kulmala[1,2], Yujing Mu[3], Hong He[3]

[1] Aerosol and Haze Laboratory, Advanced Innovation Center for Soft Matter Science and Engineering, Beijing University of Chemical Technology, Beijing, 100029, China

[2] Institute for Atmospheric and Earth System Research, Faculty of Science, University of Helsinki, Helsinki, 00014, Finland

[3] State Key Joint Laboratory of Environment Simulation and Pollution Control, Research Center for Eco-Environmental Sciences, Chinese Academy of Sciences, Beijing, 100085, China

[4] Beijing Convenient Environmental Tech Co. Ltd, Beijing, 101115, China

[5] College of Chemistry and Chemical Engineering, China West Normal University, Nanchong, 637002, China

*Corresponding author: E-mail: liuyc@buct.edu.cn; Tel: +86-10-68471480

Abstract:

Since the 1960s, many indoor and outdoor smog chambers have been developed worldwide. However, most of them are made of Teflon films, which have relatively high background contaminations due to wall effect. We developed the world's first medium-size quartz chamber (10 m^3), which is jointed with 32 pieces of 5 mm thick polished quartz glasses and a stainless-steel frame. Characterizations show that this chamber exhibits excellent performance in terms of relative humidity (RH) (2-80%) and temperature (15-30 ± 1 ℃) control, mixing efficiency of reactants (6-8 min), light transmittance (>90% above 290 nm) and wall loss of pollutants. The wall loss rates of gas-phase pollutants are on the order of 10^{-4} min^{-1} at 298K under dry conditions. It is 0.08 h^{-1} for 100-500 nm particles, significantly lower than those of Teflon chambers. The photolysis rate of NO_2 (J_{NO2}) is automatically adjustable to simulate the diurnal variation of solar irradiation from 0 to 0.40 min^{-1}. The inner surface of the chamber can be repeatedly washed with deionized water, resulting into low background contaminations. Both experiments (toluene-NO*x* and α-pinene-ozone systems) and box model demonstrate that this new quartz chamber can provide high-quality data for investigating SOA and O_3 formation in the atmosphere.

Keywords: Quartz Chamber, Characterization, SOA and O_3 formation

Synopsis: A water-washable quartz chamber with low particle loss rate was constructed for simulating atmospheric chemistry under clean conditions.

1.Introduction

Air pollution is both local and global environmental issues. Many smog chambers have been developed worldwide for understanding the mechanisms of air pollution events, such as photochemical smog and secondary organic aerosol (SOA) formation under well-controlled conditions. The smog chambers are usually divided into outdoor and indoor chambers in terms of light sources. The former one uses the natural sunlight, while the latter one usually uses artificial lights.[1] Many experiments on ozone (O_3) and SOA formation have been carried out in large outdoor chambers.[2-7] However, it is a challenge to repeat experiments with the same diurnal variations of solar irradiation and temperature. In contrast, it is easy to do that by precisely controlling reaction conditions (e.g., temperature, humidity, and pressure) using an indoor chamber although the artificial light spectrum of indoor chambers differs from the solar spectrum, resulting in different rates for some photolysis reactions.[8-10]

Table S1 summarizes the worldwide outdoor and indoor chambers used to simulate the atmospheric photochemical processes. In the 1970s, the large-size smog chamber abroad was aimed to understand the formation of near-ground O_3 pollution.[11, 12] In the following thirty years, the indoor and outdoor chambers were widely used to study the general mechanism of secondary pollutants, such as ground-level-ozone[13-15] and SOA.[6, 16-19] After the 2000s, many smog chambers have been set up or transformed, rebuilt and upgraded, to deal with the issues of atmospheric chemistry, such as $PM_{2.5}$ pollution,[4, 20, 21] reaction kinetic parameters and mechanisms[22, 23] of intermediate products from volatile organic compounds (VOCs) oxidation [24-27] and multiphase processes,[28, 29] and so on. In China, chamber studies have been started to investigate gas-phase kinetics in the atmosphere in the early 1980s.[30-32] Tang et al. [33] built the

earliest indoor chamber in Peking University to disclose the photochemical smog phenomenon that occurred in Lanzhou, China. In the next decades, various-size of smog chambers were constructed to investigate a series of atmospheric issues, including the photochemical-reaction mechanism of O_3 and aerosol formation,[34-38] the primary emissions and secondary formation process of biomass,[39] gasoline and diesel exhuasts,[40-42] and physicochemical properties of SOA.[43-46]

Complex atmospheric chemical mechanisms or models, such as the Master Chemical Mechanisms (MCM),[47] the Regional Atmospheric Chemistry Mechanisms (RACM),[48] the Carbon Bond mechanisms,[49] and the SAPRC mechanisms,[50] have been developed with the help of chamber studies.[11 12 51] Nowadays, fine atmospheric chemical mechanisms, such as highly oxidized molecules (HOMs) formation,[52] new particle formation (NPF) and gas-to-particle partitioning,[53] and the reaction kinetics of important intermediates[43, 54-58] have attracted much attention in chamber studies. In particular, it is feasible for studying the formation mechanism or kinetics of intermediates with extremely low concentrations with the aid of the state-of-the-art instruments, such as high-resolution chemical ionization mass spectrometer (HR-CIMS), high-resolution time-of-flight aerosol mass spectrometer (HR-ToF-AMS) and so on. When dealing with these scientific issues, low background contamination is a new requirement for chamber studies.

So far, the smog chambers were almost made of Teflon films, including fluorinated ethylene propylene (FEP), poly tetra fluoroethylene (PTFE) and perfluoroalkoxy (PFA) .[53] The advantages of Teflon chambers include changeable shape to keep constant pressure during experiments and to be evacuated for speeding up chamber cleaning, chemical inertness for

some reactants and intermediate products, and easiness for construction.[53, 59] However, the inner walls of a Teflon reactor are easily contaminated by depositing gas-phase and particle-phase pollutants due to the electrostatic property of the Teflon film. Thus, the contamination between different experimental runs is an important problem for chamber studies. Subsequently, it requires a thorough cleaning after an experiment. Even so, Teflon reactor usually has a short lifetime, and a high cost for the film replacement. In addition, Teflon film is permeable for some trace gases and even a source of VOCs. This usually results in a relatively high background, which is a challenge for understanding the atmospheric processes under extremely clean conditions. This is one of the driven forces to construct the CLOUD chamber, CESAM [60] (4.2 m^3) and HIRAC[61] (2 m^3) with stainless-steel which is water-washable[62] and the Simulation of Atmospheric Photochemistry In a large Reaction Chamber[22] (SAPHIR) using double-layers of Teflon films. Quartz is a water-washable material with chemical inertness and high UV-light transparency. It is widely used as the material for flow tube reactors with volume usually from tens to hundreds of liters. Small size quartz chambers such as QUAREC[63] (1.08 m^3) and CERNESIM[64] (0.78 m^3) have been reported. However, the large ratio of surface area to volume (S/V) of the flow tube reactors and small chambers limits its application in photochemistry studies under the concentration conditions close to that in the ambient air. In addition, the relatively small volume, leading to a short residence time, means that it is difficult to simulate reactions with long reaction time. To our best knowledge, a large smog chamber ($V > 2$ m^3) made of quartz has not been reported yet[63-65] due to manufacture and the cost.

In this study, we described a 10 m^3 quartz indoor photochemical chamber newly built in the Aerosol and Haze Laboratory at Beijing University of Chemical and Technology

(AHL/BUCT). As the world's first medium-size quartz chamber at present, it can be cleaned with deionized water (Section 2.3) to minimize the contamination between two experiments. It also extends the life-cycle and greatly reduce the maintaining-costs compared with Teflon chambers. The AHL/BUCT chamber was designed to simulate the atmospheric photochemical processes under repeatable conditions (e.g., temperature, humidity, and light intensity). A series of experiments were performed to characterize the chamber, including homogeneity of reactants, irradiation intensity and light transmission, wall loss of gaseous and particle pollutants, and background of the chamber. In addition, the preliminary application experiments have been carried out using the classic gas-phase photochemical reaction of the toluene-NO*x* system and ozonolysis of α-pinene in the dark.

2. Instrumentation

The quartz chamber system is a laboratory simulation unit of the AHL/BUCT station, which is equipped with the state-of-the-art instruments in connection to atmospheric trace gases, aerosol particle size and mass concentrations, cluster and aerosol particle chemical composition on the levels from molecular size to micrometer size.[66] The chamber system consists of five parts, i.e., a quartz reactor, an enclosure unit along with temperature and UV irradiation controlling system, a clean unit, a pollutants-supply unit and a detecting unit (Figure 1). The quartz reactor sets in the enclosure which is temperature-controllable and is also the support of UV lights. The whole chamber system is in a temperature-conditioned room. Figure S1 shows the pictures of the reactor and the enclosure.

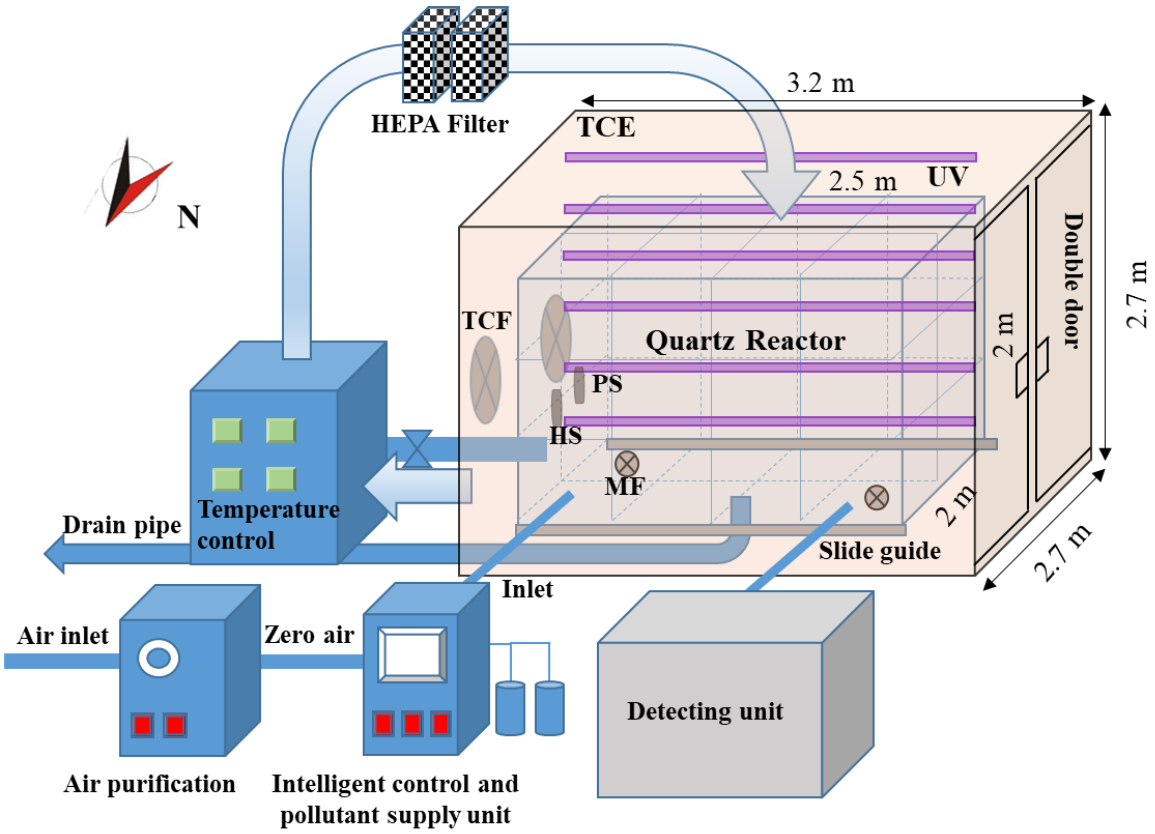

Figure 1. Schematic diagram of the AHL/BUCT quartz chamber (TCE: temperature-controlled enclosure; TCF: temperature-controlled fans; MF: magnetic fans; PS: pressure sensor; HS: humidity sensor).

Briefly, the quartz reactor is a 10 m^3 cuboid reactor, which consists of 32 pieces of polished quartz glasses (5 mm of thickness), a stainless-steel flange (30 × 100 mm) with a quartz window (165 mm I.D.) and a stainless-steel frame (2.5 × 2 × 2 m, L, W and H). Several inlets, sampling lines and a temperature and humidity sensor (HMP110, Vaisala, Finland) and a pressure sensor (MSW101, Dwyer, America) are installed inside the reactor. A cuboid enclosure (3.2 × 2.7 × 2.7 m) is temperature-conditioned through a circulation system. 60 UV lamps (1.2 m, 60 W Philips/10R PL, Germany) with the main wavelength at 371 nm are mounted on the inner wall of the enclosure. The reactor can be cleaned by both deionized water and zero-air. Water spray is introduced through the aforementioned flange with a high-pressure water gun, while the

zero-air system is the same as the that of traditional Teflon chambers. A pollutant supply unit and a detecting unit are similar to those used in the traditional chambers and described in the SI.

3. Characterization of the chamber

A series of experiments have been carried out to evaluate the performance of the quartz chamber, including the homogeneity of reactants, the light spectrum and irradiation intensity, the wall losses of gaseous pollutants and particles. All experiments are carried out at the RH lower than 10%. Only a part of instruments such as a Vocus proton transfer reaction mass spectrometry (Vocus-PTR-MS), a single photon ionization (SPI) TOF-MS (SPIMS), inorganic trace-gas analyzer, and a scanning mobility particle sizer (SMPS) are involved in these experiments.

3.1. Basic parameters

The temperature in the BUCT quartz chamber is accurately controlled in the range of 15-30 ℃ by a circulation system. The temperature in the chamber is monitored by a temperature sensor. Two fans inside the chamber ensures the homogeneity of the temperature in the reactor. Figure S2 shows the evolution of the temperature inside the chamber in the dark and in the light. The temperature of the chamber reaches a target value within 30 minutes. The fluctuation of temperature is below ±1 ℃ in the dark and below ±2 ℃ when all lights are turned on. The pressure in quartz reactor can be accurately controlled in whole experiment (Figure S3). These results indicate a good performance of temperature control inside the chamber.

NO*x* is chosen as a tracer to test the mixing time for gas-phase pollutants inside the chamber. The inlet for gas-feeding is in the middle of the chamber. The NO*x* was injected into

161 the chamber at a flow rate of 2 L min^{-1} for 3 min in each pulse from a standard gas cylinder.
162 Before the NO*x* is added, the fans are turned on. Figure S4 shows the change of NO*x*
163 concentration, which is continuously monitored using a NO*x* analyzer. The NO*x* concentration
164 becomes stable within 6-8 min after the injection. For other compounds, like toluene, a similar
165 mixing time is observed. Compared to the duration of each chamber experiment, which may
166 be several hours, this mixing time is acceptable.

167 **3.2. Light spectrum and intensity**

168 The emission spectrum of the UV lamps is measured using a spectrometer (StellarNet,
169 Inc., USA) and is shown in Figure S5. The irradiation is in the range of 340-600 nm with the
170 strongest peak at 371 nm, slightly higher than other indoor chambers (353-370 nm)[41, 67, 68].
171 Several small peaks at 300-600 nm are also observable like other UV lamps used in indoor
172 chambers [9, 35, 69]. The emission wavelength can well represent the sunlight (the light-yellow
173 filled area) in the low wavelength region. Figure S5 also shows the transmittance of the quartz
174 with 5 mm of depth (the light blue line) measured using the UV-visible spectrophotometer
175 (INESA Instrument., China). The transmittance is over 90% in the wavelength range of 290-
176 1100 nm. We also measured the transmittance of FEP Teflon film with 125 μm depth (Du Pont).
177 The transmittance decreases from around 90 % at 1100 nm to 65 % at 300 nm. At 371 nm, the
178 transmittance of the quartz and the FEP film are 91.5 % and 74.5 %, respectively. These results
179 indicate that quartz is better than FEP and is an ideal material for the smog chamber reactor as
180 far as the light transmittance is considered. The distribution of light intensity in the chamber is
181 relatively uniform (Figure S6).

182 In chamber studies, the light intensity is usually represented by the photolysis rate of NO_2

(J_{NO2}), which is estimated according to a steady state of the photochemical reaction system of NO-NO_2-O_3. NO_2 is injected into the chamber, irradiated with the UV lights. According to the monitored mixing ratio of NO, NO_2, and O_3, J_{NO2} is calculated using the flowing equation,[70]

$$J_{NO_2} = k_{NO+O_3}[NO][O_3]/[NO_2] \quad (1)$$

where $[NO]$, $[NO_2]$, and $[O_3]$ are the equilibrium concentrations (molecules cm^{-3}) of NO, NO_2 and O_3, respectively; k_{NO+O3} represents the second-order rate constant between ozone and NO reaction (1.73×10^{-14} cm^3 $molecule^{-1}$ s^{-1} at 298 K [70]). The re-equilibrium reactions among NO, NO_2 and O_3 in the sampling lines will have an influence on the measurement of their concentrations in the reactor. In this work, the J_{NO2} is calculated using a MATLAB code which accounting for the re-equilibrium in the sample lines.

The J_{NO2} is 0.40±0.01 min^{-1} when all the UV lights are turned on (full stars in Figure 2B). It decreases to 0.20±0.01 min^{-1} when a half of UV lights are turned off (open stars in Figure 2B). This shows a good linearity for the UV lights. The maximal J_{NO2} of our chamber is slightly lower than that of GIG-CAS chamber[35] (0.49 min^{-1}), while is in the range of these reported values 0.12~0.55 min^{-1} in other studies[40, 71]. The hourly mean ambient J_{NO2} (the pink line) varies from 0.005 to 0.41 min^{-1} (Figure 2A). Figure 2B shows the mean diurnal curve of J_{NO2} measured at BUCT using a photolysis rate spectrometer (2pi-j_{NO2}-Filter Radiomer, Metcon, Germany). The maximal J_{NO2} of our chamber is comparable with the ambient values at noon in summer (0.41 min^{-1}), while the J_{NO2} with a half of UV lights is close to the ambient value at noon in winter (0.20-0.25 min^{-1}). The calculated JO1D[72] with all light on is about 0.75×10^{-4} min-1, which is comparable with the ambient values ($1.2\sim3\times10^{-4}$ min^{-1}, based on the measured spectrum) at noon in winter of Beijing, but lower than that ($6\sim1.8\times10^{-4}$ min^{-1}) in summer

Beijing. In addition, the lamps can be automatically controlled with a program. As shown in Figure 2B (the blue dots and lines), the light system can well simulate the diurnal curve of ambient J_{NO2} based on the linear correlation of J_{NO2} and lamp number. This indicates that the BUCT chamber can simulate the photochemistry in a day and in different seasons in Beijing.

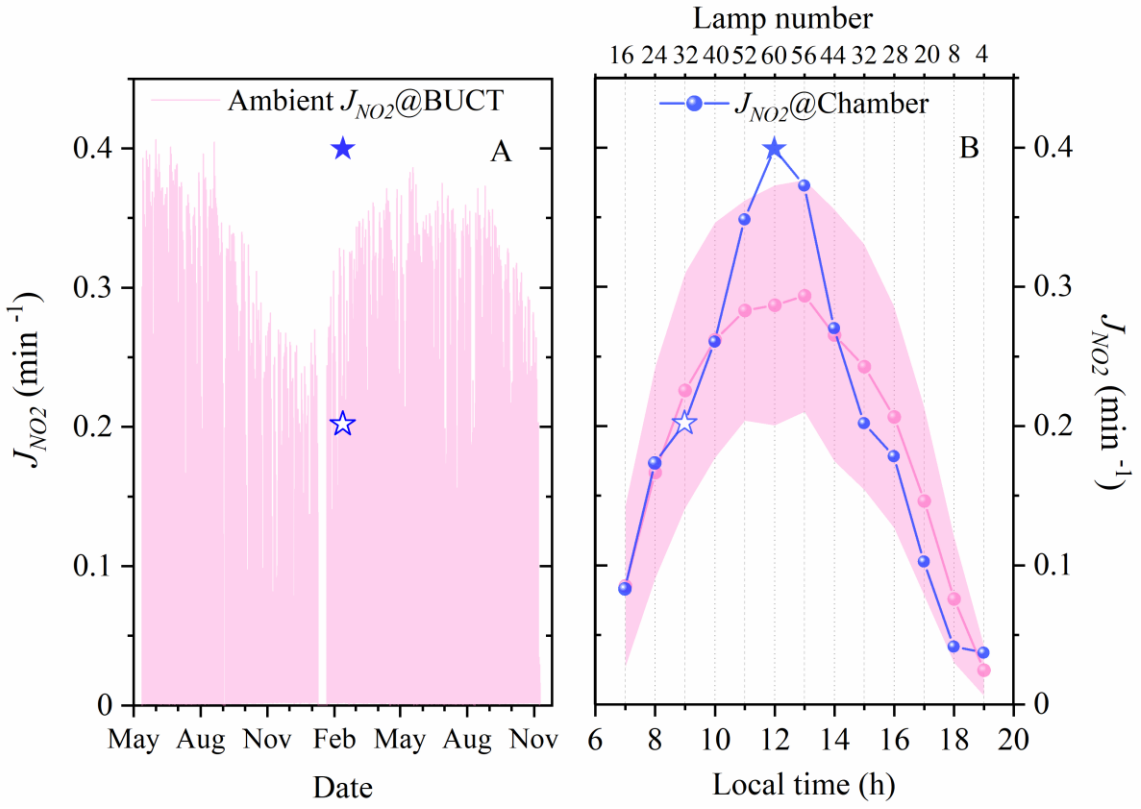

Figure 2. Comparison of J_{NO2} between BUCT chamber and ambient data (The full star means the J_{NO2} when all lights are turned on and the hollow star means that when a half lights are turned on, the purple lines and filled area denote the ambient J_{NO2} measured at BUCT).

3.3. Wall loss of typical gas species and particles

Wall loss rate is a key parameter in chamber studies. The wall loss rates of NO, NO_2 and O_3, which has been widely reported in literatures, were investigated by injecting a certain concentration of the corresponding gas and presented in their first-order decay rates in the dark. Table S3 shows the wall loss rates of O_3, NO and NO_2 in our chamber. They were

6.76~8.90×10^{-4}, 4.50~4.58×10^{-4}, and 2.16~3.54×10^{-4} min^{-1}, respectively. Compared with other chambers reported in the literatures,[5, 25, 35, 41, 73] the wall loss rates of these gas species in our chamber are higher than others (see Table S3) because our chamber has a larger ratio of surface-to-volume area (*S/V*=2.6 m^{-1}). The wall loss rate of toluene ((0.11-0.46) ×10^{-4} min^{-1}) in our chamber is one order of magnitude smaller than the value ((2.20±0.39)×10^{-4} min^{-1}) in RCEES chamber [74]. This shows the different adsorptive properties for the quartz and stainless-steel frame compared with Teflon films. In addition, the wall loss rates of intermediates range from 10^{-5} to 10^{-4} min^{-1} (Table S4), which means they are acceptable during the typical 6-hour photochemical experiments.

Particles can deposit to the reactor walls due to turbulence, Brownian diffusion, gravitational settling, and electrostatic deposition. The wall losses of particles are usually treated as a first-order process. Thus, the loss rate, k_{dep}, is expressed as the following equation,

$$\frac{dN(d_p,t)}{dt} = -k_{dep}(d_p)N(d_p,t) \quad (2)$$

where $N(d_p,t)$ is the particle number concentration at a certain particle diameter (d_p).[75] Ammonium sulfate ($(NH_4)_2SO_4$) seed particles were used as the reference aerosol to measure the particle wall losses. About 0.05 mol L^{-1} of $(NH_4)_2SO_4$ solution was atomized with a flow rate of 2 L min^{-1} zero air. Then, it was dried through a diffusion dryer filled with silica gels to remove the water before introducing into the reactor. The total number concentration of $(NH_4)_2SO_4$ was in the range of 2000~3000 molecule cm^{-3} to reduce the coagulation of particles in the chamber. For a cuboid chamber, the dependence of the wall loss rate on particle diameter can be described according to equation (3),[8]

$$k_{dep} = a \times d_p^b + c \times d_p^d \quad (3)$$

where the parameters (*a*, *b*, *c*, and *d*) are 2.66×10^{-6}, 1.76, 15.23 and -1.36, respectively. These parameters are comparable with literature data.[5, 76] Figure S7 shows wall loss rate of $(NH_4)_2SO_4$ particles as a function of particle diameter. The k_{dep} is in the range of 0.02~0.24 h^{-1}. For particles with d_p less than 100 nm, the loss rates decrease with the d_p increasing. When the d_p is greater than 100 nm, it increases as the d_p increasing. Diffusion deposition greatly contributes to the wall loss of small particles when the particle diameter is less than 50 nm, while gravitational settling leads to quick deposition of large particles. This is similar to these previous studies.[5 40] Table S5 compares the overall k_{dep} (100-500 nm) among different chambers. It is 0.08 h^{-1} in our chamber, and this corresponds to a lifetime of 12.5 h. Although the volume of our chamber is smaller than other FEP Teflon chambers, the k_{dep} value of our chamber is lower than other chambers (0.12-0.40 h^{-1}), while it is lightly higher than the glass coated stainless steel (0.028 h^{-1}) [77] and CESAM stainless steel chamber (0.01 h^{-1}) [60]. This should be mainly because of the different materials of the reactors. For our chamber, the stainless-steel frames are electrostatics-proof material. In addition, the specific resistivity of quartz is 5×10^{16}-7.5×10^{17} Ω m[78], while it is $>1\times10^{18}$ Ω m for Teflon film[79]. This implies a slight weaker dielectric potential of quartz than FEP Teflon.

3.4. Quartz reactor cleanliness

Long-term experiments will result in inorganic and organic contaminants depositing on the inner wall of the smog chamber. Thus, it is important to minimize the contamination between two experimental runs. The chamber was progressively cleaned by two methods:1) cleaning cycles involving zero air in the presence of UV light; 2) continuously flushing with deionized water.

In the chamber testing period, aerosol bursts characterized by large peak concentrations (>10000 cm^{-3}) usually occurred among 6-weeks experimental runs. After every experiment, the air flow rate was maintained at 40 L min^{-1}, which means the chamber was flushed with 6 times of the chamber volumes zero air per day. After that, the particle mass concentration was less than 0.01 μg m^{-3}. However, contaminants, from deposited organic vapors and particles, are a potential source of backgrounds which may participant in the photochemistry, and aerosol nucleation and growth. To evaluate the performance for the water-cleaning system, we washed the chamber with deionized water. Figure S8 shows the mass spectra of H_3O^+ charged ions within m/z 12~300 Th before and after flushing the inner walls of the quartz reactor with deionized water. The signals are obviously decreased after water flushing experiment compared with that before. Figure 3 further shows the variation of SOA mass concentrations in background experiments with UV lights on before and after water-flushing. In a flow experiment mode (30 L min^{-1} of zero air flow, the light-pink highlighted area), no NPF event was observable neither before nor after water-flushing. However, in a batch mode (0 L min^{-1} of zero air flow, the light-green highlighted area), NPF event happened before water-flushing and the SOA mass concentration is up to 0.5 μg m^3 for 6h of UV irradiation. After water-flushing, the SOA concentration increased slightly in the first three hour, and the mass concentration was around 0.05 μg m^3. These results indicate that flushing with deionized water can effectively remove not only inorganic substances, but also water-soluble organics to get the lower background contamination.

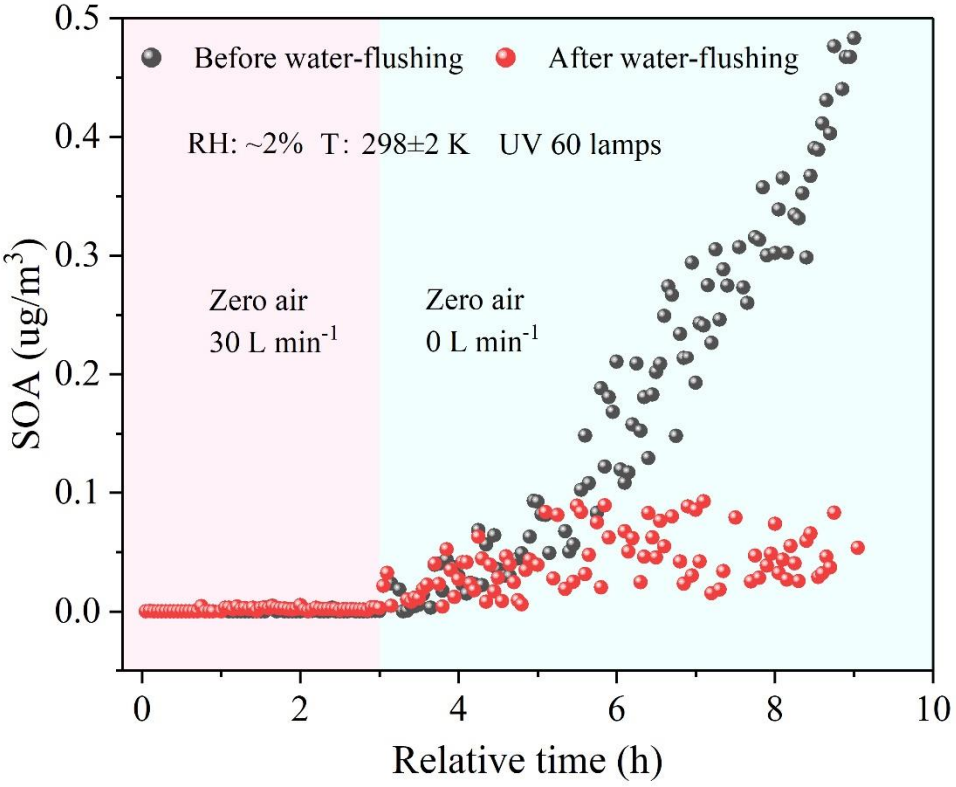

Figure 3. The variation of SOA mass concentration in the presence of UV light before and after water-flushing (the zero-air flow rate of 30 L min^{-1} in the light-pink filled area and 0 L min^{-1} in the light-green filled area, respectively)

4. Applications of the chamber in O_3 and SOA formation studies

4.1. Photochemical oxidation of toluene-NO*x* system

The toluene-NO*x* photochemical experiments were carried out to evaluate the performance of our chamber for chemical mechanism study, which has been intensively studied in other chambers.[8, 80] Four experiments have been carried out under dry conditions at 298±1 K. Table S6 summaries the initial experimental conditions. The initial toluene concentration varied from 155 to 250 ppb, and the initial toluene/NO*x* ratios (ppbC/ppb) ranged from 4.5 to

12.6. A slight over pressure was kept to prevent the ingress of air outside the chamber during our experiments.

Figure S9 shows typical profiles of different pollutants under irradiating condition. The variations of all the pollutants are the same as the classical photochemistry of VOCs-NO system. In this experiment, the initial concentration of toluene and NO*x* is 155 ppb and 86.7 ppb, respectively. The decay of toluene and NO and the formation of O_3 speeds up after ~40 min, suggesting that HONO is consumed and OH radicals (Figure S10) are vigorously generated through recycling via NO*x*/HO*x* chemistry. However, an obvious time lag (~1 h) of aerosol growth is observed in Figure S9B because of the induction duration of low volatile organic compounds (LVOCs). This is also as the same as that observed in other studies. [81]

A near-explicit mechanism of the toluene from Master Chemical Mechanism (MCM) version 3.3.1 is applied to simulate the toluene-NO photochemistry using the Framework for 0-D Atmospheric Modeling (F0AM).[82] The description of F0AM in details can be seen in supporting material (S2). In the model, the wall loss rates of NO, NO_2, and O_3 obtained in section 3.3 have been accounted for. The formation of HONO from heterogenous reactions of NO_2 on the wall surfaces has also been incorporated. Figure 4 shows the observed and simulated concentration profiles of toluene, NO, NO_2 and O_3. The modelled concentrations of toluene, NO, NO_2, and O_3 are generally well in agreement with the corresponding observed values. At the end of the experiment, toluene and O_3 is slightly overpredicted with a relative deviation of 6.7 % and 7.4 %, respectively, while NO_2 is slightly underpredicted about 6.2 %.

The quantity $\Delta([O_3]\text{-}[NO])$ is widely used to evaluate the model performance,[9, 83] which is defined as,

316 $$\Delta([O_3] - [NO]) = ([O_3]_{final} - NO_{final}) - ([O_3]_0 - [NO]_0) \quad (4)$$

317 where NO_0 and $[O_3]_0$ are the initial concentrations of NO and O_3, while NO_{final} and $[O_3]_{final}$ are

318 those at the end of experiment. $\Delta([O_3]\text{-}[NO])$ represents the amounts of NO oxidized and O_3

319 formed in the experiments, and gives an indication of the biases in simulation O_3 formation.

320 Based on the four independent experiments, the bias varies from -21.2 to 22.9 %, which is

321 within the values ±25 % reported by Carter et al (2005) [9] and Wang et al (2014) [35] for VOC-

322 NO*x* systems. Therefore, these results indicate that the AHL/BUCT chamber is suitable for

323 photochemical mechanism evaluations.

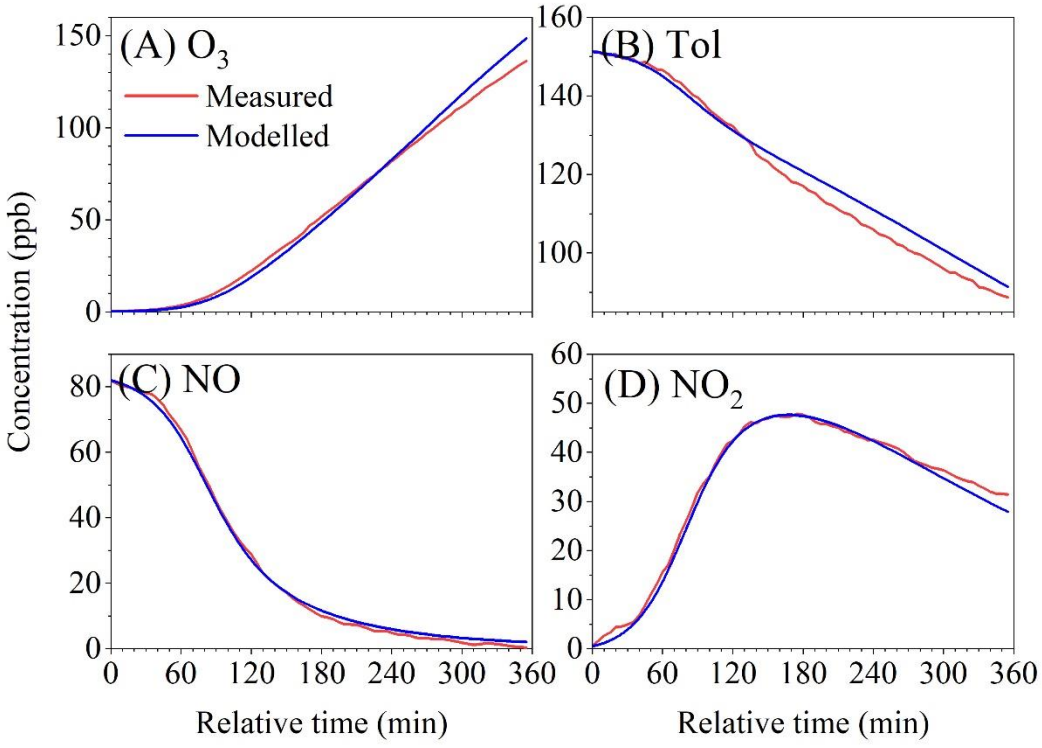

324

325 **Figure 4.** Concentration-time profiles of observed and simulated (A) ozone, (B) toluene, (C)

326 NO, and (D) NO_2 in the toluene-NO*x* experiment.

327 In addition, the SOA formation was studied in the toluene-NO*x* irradiation system. The

328 aerosol yield, *Y*, is defined as the fraction of the reacted organic gas (ROG) according to the

following equation,[18]

$$Y = \frac{\Delta M_O}{\Delta ROG} \quad (5)$$

where ΔM_O is the total mass concentration of organic aerosol formed from photochemical reactions and ΔROG is the consumed mass concentration of VOCs. Assuming aerosol density of 1.45 g cm^{-3}, which is equal to 1.45 g cm^{-3} for toluene-SOA reported by Ng et al (2007),[80] we convert the measured volume concentrations of SOA using a SMPS into mass concentrations after the wall losses of particles have been accounted for. Figure S11 compares the SOA yields of this work with previous studies. The measured SOA yields of the toluene-NO system are in the range of 0.016 to 0.097, which are comparable with the yields of 0.039 to 0.127 reported by Odum et al(1997),[18] Takekawa et al (2003),[8] Ng et al (2007),[80] and Chu et al (2012).[84]

According to partition model, Y is nonlinearly correlated to the mass concentration of organic aerosols (M_O),

$$Y = M_O \sum \frac{\alpha_i K_{om,i}}{1+K_{om,i}M_O} \quad (6)$$

Where α_i and $K_{om,i}$ are the mass-based stoichiometric coefficient and partitioning coefficient of the species i, respectively; M_O is the total mass concentration of organic aerosols. Odum et al (1996)[18] found that a two-product model can well fit the SOA yield in chamber studies. The α_1, α_2, $K_{om,1}$ *and* $K_{om,2}$ is 0.1240, 0.06623, 0.04255, and 0.006476, respectively. Table S7 summaries these four parameters reported in literatures. The α_1, $K_{om,1}$ and $K_{om,2}$ fall in the same range, and α_2 is slightly smaller than other studies indicating that the production of more low-volatility products due to the lower wall loss rate. [81]

4.2. Ozonolysis of α-pinene

Ozonolysis of α-pinene was further carried out in the dark to evaluate the flexibility of the

chamber in dark chemistry studies. This reaction has been widely studied and numerous data are available in the literature.[16, 19, 35, 75, 85] The experimental conditions are listed in the Table S8. The initial concentration of α-pinene varied from 44 to 92 ppb. The aerosol density was assumed to be 1.3 g cm^{-3} when converting the volume concentration into the mass concentration. This is equal to that of 1.3 g cm^{-3} used by Bahreini et al (2005)[86] or Alfarra et al (2006), [87] but higher than that of 1.0 g cm^{-3} reported by Wang et al (2014)[35] or Li et al (2021)[5] for α-pinene SOA.

Figure 5 compares the yields of this work and previous studies under the similar conditions, i.e., experiments under dry condition, seed-free, and in the absence of OH scavengers. The SOA yields in this work are from 0.11 to 0.32, which are in the range (0.09~0.33) reported in previous studies.[19, 35, 85] The yield curve can be well fitted according to two-products model. The α_1, α_2, $K_{om,1}$, *and* $K_{om,2}$ is 0.4626, 0.04287, 0.0134 and 0.01124, respectively. As shown in Table S6, the values of $K_{om,1}$, and $K_{om,2}$ fall in the same range reported in literatures, while α_2 are slightly smaller than other studies, also indicating that the more low-volatile products formed in the chamber due to lower wall loss. In addition, the fitting-curve in this study is steeper than other reports. This may be resulted from the different adsorptive property for initial, intermediate and end species on different-material of the chamber and/or the distribution of oxidation products under different reaction conditions.

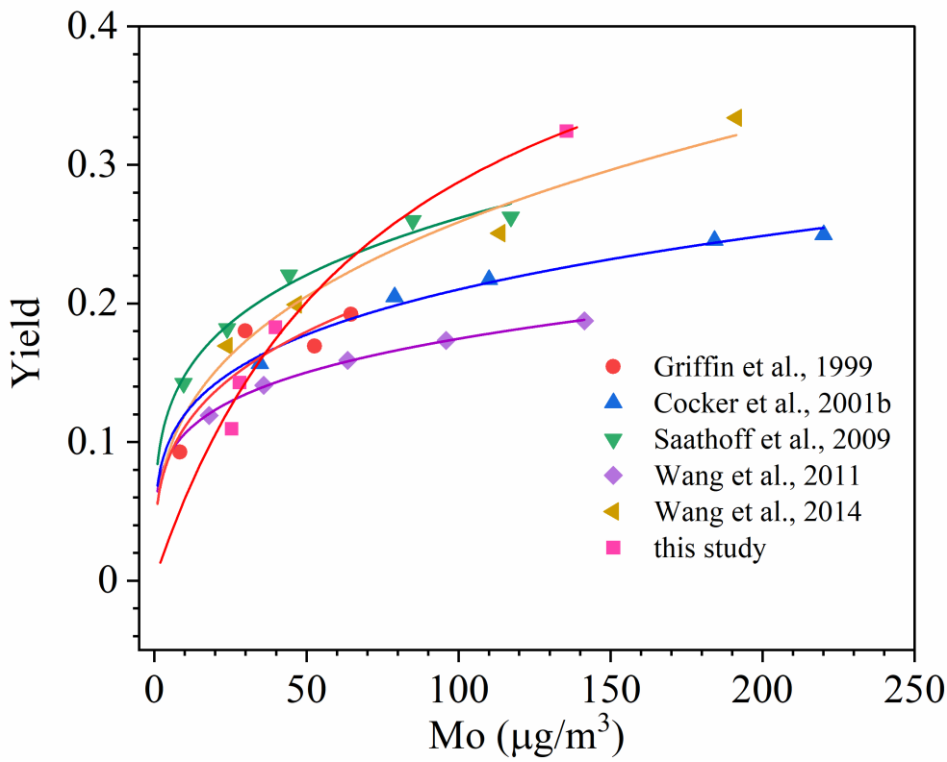

369

370 **Figure. 5** Comparison of yield data obtained for α-pinene ozonolysis experiments in BUCT

371 chamber with other chamber facilities

372 Based on full characterizations, it has been demonstrated that the BUCT chamber can be

373 used to investigate both photochemistry and atmospheric chemistry in the dark related to

374 secondary pollutants formation. Unlike traditional smog chambers made of Teflon film, the

375 quartz chamber does not need to replace the reactor periodically because the inner wall of the

376 reactor is water-washable to significantly reduce the contamination from the deposited

377 pollutants on the walls. After cleaning, the quartz chamber is particularly suitable for studying

378 atmospheric chemical mechanism and kinetics under low background conditions. Compared

379 with other no-Teflon chamber such as CLOUD chamber, the adjustable light intensity (J_{NO2})

380 makes our quartz chamber being suitable for simulating the atmospheric photochemistry in

381 different seasons and the diurnal photochemistry in Beijing. This quartz chamber also enables

382 AHL/BUCT being capable of performing field observations and laboratory simulations on the

383 transformation of gas-phase pollutants, nucleation, growth, aging and effects of atmospheric

384 aerosols at molecular, cluster, nanometer and micron level.

Supporting Information

The Supporting Information is available free of charge at

(The description of the quartz chamber; Observation-based model simulation; The worldwide smog chambers used to simulate atmospheric photochemical processes; Instruments of the AHL/BUCT quartz chamber; Comparison of gaseous pollutants wall loss rate of BUCT chamber with other chamber facilities; The wall loss rates of selected protonated intermediates; Comparison of particle wall loss rates of BUCT chamber with other chamber facilities; Experimental conditions and resulting SOA data of toluene photooxidation experiments; Four-parameters summary of two-product model used to simulate aerosol mass and yield; Experimental conditions and resulting SOA data of α-pinene ozonolysis experiments; Comparison of the wavelength region with other indoor chambers; The picture of the AHL/BUCT quartz chamber; Evolution of the temperature inside the chamber; The variation of pressure in a typical experiment; Concentration-time plot of NOx after each pulse; Measured transmittance and spectrum of 365 nm UV light; The light intensity distribution of different distances from the UV lights; Particle wall loss rate constants for different particle diameter sizes; Mass spectra of H_3O^+ charged ion measured by Vocus-PTR; The time series of the gas species and diameter in the toluene-NO*x* photochemical experiments; The variations of the concentrations of HONO and OH radical; SOA yield of toluene-NOx photochemical experiments and comparison with other chambers.)

Author Information

Corresponding Author

Yongchun Liu - *Aerosol and Haze Laboratory, Advanced Innovation Center for Soft Matter Science and Engineering, Beijing University of Chemical Technology, Beijing, 100029, China*

Authors

Wei Ma - *Aerosol and Haze Laboratory, Advanced Innovation Center for Soft Matter Science and Engineering, Beijing University of Chemical Technology, Beijing, 100029, China*

Yusheng Zhang - *Aerosol and Haze Laboratory, Advanced Innovation Center for Soft Matter Science and Engineering, Beijing University of Chemical Technology, Beijing, 100029, China*

Zemin Feng - *Aerosol and Haze Laboratory, Advanced Innovation Center for Soft Matter Science and Engineering, Beijing University of Chemical Technology, Beijing, 100029, China*

Junlei Zhan - *Aerosol and Haze Laboratory, Advanced Innovation Center for Soft Matter Science and Engineering, Beijing University of Chemical Technology, Beijing, 100029, China*

Chenjie Hua - *Aerosol and Haze Laboratory, Advanced Innovation Center for Soft Matter Science and Engineering, Beijing University of Chemical Technology, Beijing, 100029, China*

Li Ma - *Aerosol and Haze Laboratory, Advanced Innovation Center for Soft Matter Science and Engineering, Beijing University of Chemical Technology, Beijing, 100029, China*

Yishuo Guo- *Aerosol and Haze Laboratory, Advanced Innovation Center for Soft Matter Science and Engineering, Beijing University of Chemical Technology, Beijing, 100029, China*

Ying Zhang- *Aerosol and Haze Laboratory, Advanced Innovation Center for Soft Matter Science and Engineering, Beijing University of Chemical Technology, Beijing, 100029, China*

Chao Yan- *Institute for Atmospheric and Earth System Research, Faculty of Science, University of Helsinki, Helsinki, 00014, Finland*

Tianzeng Chen - *State Key Joint Laboratory of Environment Simulation and Pollution Control, Research Center for Eco-Environmental Sciences, Chinese Academy of Sciences, Beijing, 100085, China*

Qingxin Ma - *State Key Joint Laboratory of Environment Simulation and Pollution Control, Research Center for Eco-Environmental Sciences, Chinese Academy of Sciences, Beijing, 100085, China*

Chunshan Liu - *Beijing Convenient Environmental Tech Co. Ltd, Beijing, 101115, China*

Markku Kulmala - *Aerosol and Haze Laboratory, Advanced Innovation Center for Soft Matter Science and Engineering, Beijing University of Chemical Technology, Beijing, 100029, China*

Institute for Atmospheric and Earth System Research, Faculty of Science, University of Helsinki, Helsinki, 00014, Finland

Yujing Mu - *State Key Joint Laboratory of Environment Simulation and Pollution Control, Research Center for Eco-Environmental Sciences, Chinese Academy of Sciences, Beijing, 100085, China*

Hong He - *State Key Joint Laboratory of Environment Simulation and Pollution Control, Research Center for Eco-Environmental Sciences, Chinese Academy of Sciences, Beijing, 100085, China*

Notes

The authors declare no competing financial interest.

Acknowledgments

This research was financially supported by the Strategic Priority Research Program of Chinese Academy of Sciences and Beijing University of Chemical Technology, the National Natural Science Foundation of China (41877306, 92044301), the Ministry of Science and Technology of the People's Republic of China (2019YFC0214701). We also thank Beijing Convenient Environmental Tech Co. Ltd. for constructing the chamber.

References

(1). Seakins, P. W., A brief review of the use of environmental chambers for gas phase studies of kinetics, chemical mechanisms and characterisation of field instruments. *EPJ Web Conf.* **2010,** *9*, 143-163.

(2). Jennifer; E.; Stern; Richard; C.; Flagan; Daniel.; Grosjean; John; H., Aerosol formation and growth in atmospheric aromatic hydrocarbon photooxidation. *Environ. Sci. Technol.* **1987,** *21*, (12), 1224–1231.

(3). Pandis, S. N.; Paulson, S. E.; Seinfeld, J. H.; Flagan, R. C., Aerosol formation in the photooxidation of isoprene and β-pinene. *Atmos.Environ.* **1991,** *25*, (5), 997-1008.

(4). Johnson, D.; Jenkin, M. E.; Wirtz, K.; Martin-Reviejo, M., Simulating the Formation of Secondary Organic Aerosol from the Photooxidation of Toluene. *Environ. Chem.* **2004,** *2*, 35-48.

(5). Li, J.; Li, H.; Wang, X.; Wang, W.; Liu, Y., A large-scale outdoor atmospheric simulation smog chamber for studying atmospheric photochemical processes: Characterization and preliminary application. *J. Environ. Sci.* **2021,** *102*, (5), 185-197.

(6). Martin-Reviejo, M., Wirtz, K Is benzene a precursor for secondary organic aerosol? *Environ. Sci. Technol.* **2005,** *39*, (4), 1045-54.

(7). Rollins, A. W.; Kiendler-Scharr, A.; Fry, J. L.; Brauers, T.; Brown, S. S.; Dorn, H. P.; Dubé, W.; Fuchs, H.; Mensah, A.; Mentel, T. F., Isoprene oxidation by nitrate radical: alkyl nitrate and secondary organic aerosol yields. *Atmos. Chem. Phys.* **2009,** *9*, (2).

(8). Takekawa, H. M., H. Yamazaki, S., Temperature dependence of secondary organic aerosol formation by photo-oxidation of hydrocarbons. *Atmos.Environ.* **2003,** *37*, (24), 3413-3424.

(9). Carter, W.; Iii, D.; Fitz, D. R.; Malkina, I. L.; Bumiller, K.; Sauer, C. G.; Pisano, J. T.; Bufalino, C.; Song, C., A new environmental chamber for evaluation of gas-phase chemical mechanisms and secondary aerosol formation. *Atmos.Environ.* **2005,** *39*, (40), 7768-7788.

(10). Paulsen; Dommen; Kalberer; Prevot; ASH; Richter; Sax; Steinbacher; Weingartner; Baltensperger, Secondary organic aerosol formation by irradiation of 1,3,5-trimethylbenzene-NOx-H_2O in a new reaction chamber for atmospheric chemistry and physics. *Environ. Sci. Technol.* **2005,** *39*, (8), 2668-78.

(11). Akimoto, H.; Hoshino, M.; Inoue, G.; Sakamaki, F.; Washida, N.; Okuda, M., Design and characterization of the evacuable and bakable photochemical smog chamber. *Environ. Sci. Technol.* **1979,** *13*, (4), 471-475.

(12). Carter, W., Atkinson, R. Winer, A. M., Experimental investigation of chamber-dependent radical sources. *Int. J. Chem. Kinet.* **1982,** *14*, (10), 1071-1103.

(13). Dodge, M. C., Chemical oxidant mechanisms for air quality modeling: critical review. *Atmos.Environ.* **2000,** *34*, (12-14), 2103-2130.

(14). Hess, G. D.; Carnovale, F.; Cope, M. E.; Johnson, G. M., The evaluation of some photochemical smog reaction mechanisms—I. Temperature and initial composition effects. *Atmos.Environ.* **1992,** *26*, (4), 625-641.

(15). Simonaitis, R.; Meagher, J. F.; Bailey, E. M., Evaluation of the condensed carbon bond (CB-IV) mechanism against smog chamber data at low VOC and NOx concentrations. *Atmos.Environ* **1997,** *31*, (1), 27–43.

(16). Griffin, R. J.; Cocker, D. R.; Flagan, R. C.; Seinfeld, J. H., Organic aerosol formation from the oxidation of biogenic hydrocarbons. *J. Geophys. Res.: Atmos.* **1999,** *104*, 3555-3567.

(17). Mcmurry, P. H.; Grosjean, D., Gas and aerosol wall losses in Teflon film smog chambers. *Environ. Sci. Technol.* **1985,** *19*, (12), 1176.

(18). Odum, J. R.; Hoffmann, T.; Bowman, F.; Collins, D.; Flagan, R. C.; Seinfeld, J. H., Gas/Particle Partitioning and Secondary Organic Aerosol Yields. *Environ. Sci. Technol.* **1996,** *30*, (8), 2580-2585.

(19). Saathoff, H.; Naumann, K. H.; MHler, O.; Jonsson, M.; Hallquist, M.; Kiendler-Scharr, A.; Mentel, T. F.; Tillmann, R.; Schurath, U., Temperature dependence of yields of secondary organic aerosols from the ozonolysis

of α-pinene and limonene. *Atmos. Chem. Phys.* **2009,** *9*, (5), 1551-1577.
(20). M. Hallquist, J. C. W., U. Baltensperger, Y. Rudich, D. Simpson M. Claeys, J. Dommen, N. M. Donahue, C. George, A. H. Goldstein, J. F. Hamilton, H. Herrmann, T. Hoffmann, Y. Iinuma, M. Jang, M. E. Jenkin, J. L. Jimenez, A. Kiendler-Scharr, W. Maenhaut, G. McFiggans, Th. F. Mentel, A. Monod, A. S. H. Prévôt, J. H. Seinfeld, J. D. Surratt, R. Szmigielski, and J. Wildt, The formation, properties and impact of secondary organic aerosol: current and emerging issues. *Atmos. Chem. Phys.* **2009,** *9*, 5155-5236.
(21). Hurley, M.; Sokolov, O.; Wallington, T. J.; Takekawa, H.; Karasawa, M.; Klotz, B.; Barnes, I.; Becker, K. H., Organic aerosol formation during the atmospheric degradation of toluene. *Environ. Sci. Technol.* **2001,** *35*, (7), 1358-1366.
(22). Rohrer, F.; Bohn, B.; Brauers, T.; Brüning, D.; Johnen, F. J.; Wahner, A.; Kleffmann, Characterisation of the photolytic HONO-source in the atmosphere simulation chamber SAPHIR. *Atmos. Chem. Phys.* **2005,** *5*, (8), 2189-2201.
(23). Ren, Y.; Bernard, F.; Daele, V.; Mellouki, A., Atmospheric Fate and Impact of Perfluorinated Butanone and Pentanone. *Environ. Sci. Technol.* **2019,** *53*, (15), 8862-8871.
(24). Brauers, T. B., B. ; Johnen, F. -J. ; Rohrer, R. ; Rodriguez Bares, S. ; Tillmann, R. ; Wahner, A. In *The atmosphere simulation chamber SAPHIR: a tool for the investigation of photochemistry*, EGS - AGU - EUG Joint Assembly, Nice, France, April, 2004; Nice, France, 2004.
(25). Bloss, C.; Wagner, V.; Jenkin, M. E.; Volkamer, R.; Bloss, W. J.; Lee, J. D.; Heard, D. E.; Wirtz, K.; Martin-Reviejo, M.; Rea, G., Development of a detailed chemical mechanism (MCMv3.1) for the atmospheric oxidation of aromatic hydrocarbons. *Atmos. Chem. Phys.* **2004,** *5*, (3), 641-664.
(26). Bohn, B.; Rohrer, F.; Brauers, T.; Wahner, A., Actinometric measurements of NO2 photolysis frequencies in the atmosphere simulation chamber SAPHIR. *Atmos. Chem. Phys.* **2004,** *5*, (2), 493-503.
(27). Ren, Y.; Grosselin, B.; Dale, V.; Mellouki, A., Investigation of the reaction of ozone with isoprene, methacrolein and methyl vinyl ketone using the HELIOS chamber. *Faraday Discuss.* **2017,** *200*, 289-311.
(28). PaSchl, U.; Shiraiwa, M., Multiphase Chemistry at the Atmosphere–Biosphere Interface Influencing Climate and Public Health in the Anthropocene. *Chem. Rev.* **2015,** *115*, (10), 4440-75.
(29). Warneke C. J. A. de Gouw, P. D. G., W. C. Kuster,E. J. Williams,B. M. Lerner,R. Jakoubek,S. S. Brown,H. Stark,M. Aldener,A. R. Ravishankara,J. M. Roberts,M. Marchewka,S. Bertman,D. T. Sueper,S. A. McKeen,J. F. Meagher,F. C. Fehsenfeld, Comparison of daytime and nighttime oxidation of biogenic and anthropogenic VOCs along the New England coast in summer during New England Air Quality Study 2002. *J. Geophys. Res.: Atmos.* **2004,** *109*, (D10), D10309.
(30). Wang, W.; Ying, X.; Lin, Z.; Wang, H., Study on reaction rate constants of CH_4 and its life-time. *China Environ. Sci.* **1995,** *15*, (4).
(31). Ren, K.; Jianjun, L. I.; Wang, W., Investigation on experiment system for modeling of photochemical smog. *Acta Scientiae Circumstantiae* **2005,** *25*, (11), 1431-1435.
(32). Yongfu, X. U.; Jia, L.; Maofa, G. E.; Lin, D. U.; Wang, G.; Wang, D., A kinetic study of the reaction of ozone with ethylene in a smog chamber under atmospheric conditions. *Chin. Sci. Bull.* **2006,** *51*, (23), 2839-2843.
(33). Tang, X., Bi, M., Li, J., Zhang, X, Trial production and performance experiment of photochemical smog chamber. *Environ. Chem.* **1982,** *1*, 344-351.
(34). Liu, S.; Jia, L.; Xu, Y.; Tsona, N. T.; Ge, S.; Du, L., Photooxidation of cyclohexene in the presence of SO2: SOA yield and chemical composition. *Atmos. Chem. Phys.* **2017,** *17*, (21), 13329-13343.
(35). Wang, X.; Liu, T.; Bernard, F.; Ding, X.; Wen, S.; Zhang, Y.; Zhang, Z.; He, Q.; Lü, S.; Chen, J., Design and characterization of a smog chamber for studying gas-phase chemical mechanisms and aerosol formation. *Atmos. Meas. Tech.* **2014,** *7*, (1), 301-313.

(36). Shan Wu , Z. L., Jiming Hao , Zhe Zhao , Junhua Li , Hideto Takekawa, Hiroaki Minoura & Akio Yasuda Construction and Characterization of an Atmospheric Simulation Smog Chamber. *Advances in Atmospheric Sciences* **2007,** *02*, 90-98.
(37). Li, K.; Chen, L.; White, S. J.; Hai, Y.; Cen, K., Smog chamber study of the role of NH3 in new particle formation from photo-oxidation of aromatic hydrocarbons. *Sci. Total Environ.* **2018,** *619-620*, 927.
(38). Isaacman-VanWertz, G.; Massoli, P.; O'Brien, R.; Lim, C.; Franklin, J. P.; Moss, J. A.; Hunter, J. F.; Nowak, J. B.; Canagaratna, M. R.; Misztal, P. K.; Arata, C.; Roscioli, J. R.; Herndon, S. T.; Onasch, T. B.; Lambe, A. T.; Jayne, J. T.; Su, L.; Knopf, D. A.; Goldstein, A. H.; Worsnop, D. R.; Kroll, J. H., Chemical evolution of atmospheric organic carbon over multiple generations of oxidation. *Nat Chem* **2018,** *10*, (4), 462-468.
(39). Zhang, H.; Hu, D.; Chen, J.; Ye, X.; Wang, S. X.; Hao, J. M.; Lin, W.; Zhang, R.; An, Z., Particle Size Distribution and Polycyclic Aromatic Hydrocarbons Emissions from Agricultural Crop Residue Burning. *Environ. Sci. Technol.* **2011,** *45*, (13), 5477-5482.
(40). Chen, T.; Liu, Y.; Liu, C.; Liu, J.; Chu, B.; He, H., Important role of aromatic hydrocarbons in SOA formation from unburned gasoline vapor. *Atmos.Environ.* **2019,** *201*, (MAR.), 101-109.
(41). Chen, T.; Liu, Y.; Ma, Q.; Chu, B.; He, H., Significant source of secondary aerosol: formation from gasoline evaporative emissions in the presence of SO2 and NH3. *Atmos. Chem. Phys.* **2019,** *19*, (12), 8063-8081.
(42). Kamens, R. M.; Zhang, H.; Chen, E. H.; Yang, Z.; Parikh, H. M.; Wilson, R. L.; Galloway, K. E.; Rosen, E. P., Secondary organic aerosol formation from toluene in an atmospheric hydrocarbon mixture: Water and particle seed effects. *Atmos.Environ.* **2011,** *45*, (13), 2324-2334.
(43). Li, J. L., K. Wang, W. Wang, J. Peng, C. Ge, M., Optical properties of secondary organic aerosols derived from long-chain alkanes under various NOx and seed conditions. *Sci. Total Environ.* **2017,** *579*, 1699-1705.
(44). Li, J.; Wang, W.; Li, K.; Zhang, W.; Ge, M., Temperature Effects on Optical Properties and Chemical Composition of Secondary Organic Aerosol Derived from n -Dodecane. *Atmos. Chem. Phys.* **2020,** *20*, 8123-8137.
(45).Chao, P.; Wang, W.; Li, K.; Li, J.; Ge, M. F., The Optical Properties of Limonene Secondary Organic Aerosols: The Role of NO3, OH, and O3 in the Oxidation Processes. *J. Geophys. Res.: Atmos.* **2018,** *123*, (6), 3292-3303.
(46). Zhang, W.; Wang, W.; Li, J.; Peng, C.; Ge, M. F., Effects of SO2 on optical properties of secondary organic aerosol generated from photooxidation of toluene under different relative humidity. *Atmos. Chem. Phys.* **2019,** *20*, 4447-4492.
(47). Jenkin, M. E.; Saunders, S. M.; Wagner, V.; Pilling, M. J., Protocol for the development of the Master Chemical Mechanism, MCM v3 (Part A): tropospheric degradation of non-aromatic volatile organic compounds. *Atmos. Chem. Phys.* **2003,** *3*, (1), 181-193.
(48). Stockwell, W. R.; Kirchner, F.; Kuhn, M.; Seefeld, S., A new mechanism for regional atmospheric chemistry modeling. *J. Geophys. Res.: Atmos.* **1997,** *102*, (D22).
(49). White, S. J.; Azzi, M.; Angove, D. E.; Jamie, I. M., Modelling the photooxidation of ULP, E5 and E10 in the CSIRO smog chamber. *Atmos.Environ.* **2010,** *44*, (40), 5375-5382.
(50). Carter, W.; Heo, G., Development of revised SAPRC aromatics mechanisms. *Atmos.Environ.* **2013,** *77*, 404–414.
(51). Jeffries, H. E.; Sexton, K. G.; Kamens, R. M.; Holleman, M. S., Outdoor Smog Chamber Experiments to Test Photochemical Models: Phase II. *EPA* **1982,** *600*, 83-85.
(52). Bianchi, F.; Kurten, T.; Riva, M.; Mohr, C.; Rissanen, M. P.; Roldin, P.; Berndt, T.; Crounse, J. D.; Wennberg, P. O.; Mentel, T. F.; Wildt, J.; Junninen, H.; Jokinen, T.; Kulmala, M.; Worsnop, D. R.; Thornton, J. A.; Donahue, N.; Kjaergaard, H. G.; Ehn, M., Highly Oxygenated Organic Molecules (HOM) from Gas-Phase Autoxidation Involving Peroxy Radicals: A Key Contributor to Atmospheric Aerosol. *Chem. Rev.* **2019,** *119*, (6), 3472-3509.
(53). Chu, B.; Chen, T.; Liu, Y.; Ma, Q.; Mu, Y.; Wang, Y.; Ma, J.; Zhang, P.; Liu, J.; Liu, C. J. N. S. R., Application

583 of smog chambers in atmospheric process studies. **2021**.
584 (54). Knox, J. H., A new mechanism for the low temperature oxidation of hydrocarbons in the gas phase. *Combust.*
585 *Flame.* **1965,** *9*, (3), 297-310.
586 (55). Mcfiggans, G.; Mentel, T. F.; Wildt, J.; Pullinen, I.; Kang, S.; Kleist, E.; Schmitt, S.; Springer, M.; Tillmann,
587 R.; Wu, C., Secondary organic aerosol reduced by mixture of atmospheric vapours. *Nature* **2019,** *565*, (7741),
588 587-593.
589 (56). Zhou, C.; Jang, M.; Yu, Z., Simulation of SOA formation from the photooxidation of monoalkylbenzenes in
590 the presence of aqueous aerosols containing electrolytes under various NO x levels. *Atmos. Chem. Phys.* **2019,** *19*,
591 (8), 5719-5735.
592 (57). Kun Li, J. L., John Liggio, Weigang Wang,Maofa Ge, Qifan Liu, Yucong Guo, Shengrui Tong, Jiangjun Li,
593 Chao Peng, Bo Jing, Dong Wang, and Pingqing Fu, Enhanced Light Scattering of Secondary Organic Aerosols by
594 Multiphase Reactions *Environ. Sci. Technol.* **2017,** *51*, (3), 1285-1292.
595 (58). Vasquez, K. T.; Crounse, J. D.; Schulze, B. C.; Bates, K. H.; Wennberg, P. O., Rapid hydrolysis of tertiary
596 isoprene nitrate efficiently removes NOx from the atmosphere. *Proc. Natl. Acad. Sci.* **2020,** *117*, (52), 33011-
597 33016.
598 (59). Finlaysonpitts, B.; Pitts, J. J., *Chemistry of the Upper and Lower Atmosphere*. Chemistry of the upper and
599 lower atmosphere: 2000.
600 (60). Wang, J.; Doussin, J. F.; Perrier, S.; Perraudin, E.; Katrib, Y.; Pangui, E.; Picquet-Varrault, B., Design of a
601 new multi-phase experimental simulation chamber for atmospheric photosmog, aerosol and cloud chemistry
602 research. *Atmos. Meas. Tech.* **2011,** *4*, (11), 2465-2494.
603 (61). Glowacki, D. R.; Goddard, A.; Hemavibool, K.; Malkin, T. L.; Commane, R.; Anderson, F.; Bloss, W. J.;
604 Heard, D. E.; Ingham, T.; Pilling, M. J.; Seakins, P. W., Design of and initial results from a Highly Instrumented
605 Reactor for Atmospheric Chemistry (HIRAC). *Atmos. Chem. Phys.* **2007,** *7*, (20), 5371-5390.
606 (62). Jasper Kirkby, J. C., João Almeida, Eimear Dunne, Jonathan Duplissy, Sebastian Ehrhart, Alessandro
607 Franchin, Stéphanie Gagné, Luisa Ickes, Andreas Kürten, Agnieszka Kupc, Axel Metzger, Francesco Riccobono,
608 Linda Rondo, Siegfried Schobesberger, Georgios Tsagkogeorgas, Daniela Wimmer, Antonio Amorim, Federico
609 Bianchi, Martin Breitenlechner, André David, Josef Dommen, Andrew Downard, Mikael Ehn, Richard C. Flagan,
610 Stefan Haider, Armin Hansel, Daniel Hauser, Werner Jud, Heikki Junninen, Fabian Kreissl, Alexander Kvashin,
611 Ari Laaksonen, Katrianne Lehtipalo, Jorge Lima, Edward R. Lovejoy, Vladimir Makhmutov, Serge Mathot, Jyri
612 Mikkilä, Pierre Minginette, Sandra Mogo, Tuomo Nieminen, Antti Onnela, Paulo Pereira, Tuukka Petäjä, Ralf
613 Schnitzhofer, John H. Seinfeld, Mikko Sipilä, Yuri Stozhkov, Frank Stratmann, Antonio Tomé, Joonas Vanhanen,
614 Yrjo Viisanen, Aron Vrtala, Paul E. Wagner, Hansueli Walther, Ernest Weingartner, Heike Wex, Paul M. Winkler,
615 Kenneth S. Carslaw, Douglas R. Worsnop, Urs Baltensperger & Markku Kulmal, Role of sulphuric acid, ammonia
616 and galactic cosmic rays in atmospheric aerosol nucleation. *Nature* **2011,** *476*, (7361), 7251-62.
617 (63). Barnes, I.; Becker, K. H.; Mihalopoulos, N., An FTIR product study of the photooxidation of dimethyl
618 disulfide. *J. Atmos. Chem.* **1994,** *18*, (3), 267-289.
619 (64). Roman, C., Arsene, C., Bejan, I. G., and Olariu, R.-I, Investigations on the gas-phase photolysis and OH
620 radical kinetics of nitrocatechols: Implications of intramolecular interactions on their atmospheric behavior. *Atmos.*
621 *Chem. Phys. Discuss.* **2021**, 553.
622 (65). Nie, J. S.; Min, Q.; Yang, Y.; Zhang, W. J., The structure and performance of a kind of photo chemical smog
623 chamber. *Chin. J. At. Mol. Phys.* **2002,** *2002*, (02), 186-90.
624 (66). Liu, Y.; Yan, C.; Feng, Z.; Zheng, F.; Fan, X.; Zhang, Y.; Li, C.; Zhou, Y.; Lin, Z.; Guo, Y.; Zhang, Y.; Ma,
625 L.; Zhou, W.; Liu, Z.; Wei, Z.; Dada, L.; Dallenbach, K. R.; Kontkanen, J.; Cai, R.; Chan, T.; Chu, B.; Du, W.;
626 Yao, L.; Wang, Y.; Cai, J.; Kangasluoma, J.; Kokkonen, T.; Kujansuu, J.; Rusanen, A.; Deng, C.; Fu, Y.; Yin, R.;

Li, X.; Lu, Y.; Liu, Y.; Lian, C.; Yang, D.; Wang, W.; Ge, M.; wang, Y.; Worsnop, D.; Junninen, H.; He, H.; Kerminen, V. M.; Zheng, J.; Wang, L.; Jiang, J.; Petäjä, T.; Bianchi, F.; Kulmala, M., Continuous and Comprehensive Atmospheric Observations in Beijing: A Station to Understand the Complex Urban Atmospheric Environment. *Big Earth Data* **2020,** *4*, (3), 295-321.

(67). Lane, D. A. T., H., Photochemical Degradation of Polycyclic Aromatic Compounds. I. Naphthalene. Polycyclic Aromatic Compounds. *Polycyclic Aromat. Compd.* **1995,** *5*, (1-4), 131-138.

(68). Thüner, L. P. B., P.; Rea, G. J.; Wenger, J. C., Kinetics of the gas-phase reactions of OH and NO3 radicals with dimethylphenols. *J. Phys. Chem. A.* **2004,** *108*, 11019-11025.

(69). Donahue; N., M.; Henry; K., M.; Mentel; T., F.; Kiendler-Scharr; Spindler; Bohn; Brauers, Aging of biogenic secondary organic aerosol via gas-phase OH radical reactions. *P. Natl. Acad. Sci.,* **2012,** *109*, 13503-13508.

(70). Atkinson, R.; Baulch, D. L.; Cox, R. A.; Crowley, J. N.; Hampson, R. F.; Hynes, R. G.; Jenkin, M. E.; Rossi, M. J.; Troe, J., Evaluated kinetic and photochemical data for atmospheric chemistry: Volume I - gas phase reactions of Ox, HOx, NOx and SOx species. *Atmos. Chem. Phys.* **2004,** *4*, (6), 1461-1738.

(71). Li, K.; Chen, L.; Han, K.; Lv, B.; Bao, K.; Wu, X.; Gao, X.; Cen, K., Smog chamber study on aging of combustion soot in isoprene/SO2/NOx system: Changes of mass, size, effective density, morphology and mixing state. *Atmos. Res.* **2017,** *184*, (feb.), 139-148.

(72). Shetter, R. E., Davidson, J.A., Cantrell, C.A., Burzynski, N.J., Calvert, J.G., Temperature dependence of the atmospheric photolysis rate coefficient for NO_2. *J. Geophys. Res.: Atmos.* **1988,** *93*, 7113-7118.

(73). Metzger, A.; Dommen, J.; Gaeggeler, K.; Duplissy, J.; Prevot, A.; Kleffmann, J.; Elshorbany, Y.; Wisthaler, A.; Baltensperger, U., Evaluation of 1,3,5 trimethylbenzene degradation in the detailed tropospheric chemistry mechanism, MCMv3.1, using environmental chamber data. *Atmos. Chem. Phys.* **2008,** *8*, (21), 6453-6468.

(74). Chen, T.; Chu, B.; Ma, Q.; Zhang, P.; Liu, J.; He, H., Effect of relative humidity on SOA formation from aromatic hydrocarbons: Implications from the evolution of gas- and particle -phase species. *Sci. Total Environ.* **2021,** *773*.

(75). Cocker, D. R.; Flagan, R. C.; Seinfeld, J. H., State-of-the-art chamber facility for studying atmospheric aerosol chemistry. *Environ. Sci. Technol.* **2001,** *35*, (12), 2594.

(76). Liu, C.; Chu, B.; Liu, Y.; Ma, Q.; Ma, J.; He, H.; Li, J.; Hao, J., Effect of mineral dust on secondary organic aerosol yield and aerosol size in α-pinene/NOx photo-oxidation. *Atmos. Environ.* **2013,** *77*, 781-789.

(77). Izumi, K., Murano, K., Mizuochi, M., & Fukuyama, T, Aerosol formation by the photooxidation of cyclohexene in the presence of nitrogen oxides. *Environ. Sci. Technol.* **1988,** *22*, (10), 1207-1215.

(78). Bleaney, B. I. B. B., Electricity and Magnetism 3rd Edition. Great Britain. *Oxford University Press* **1976,** *63*.

(79). Nelson W. Green, A. R. F., and J. R. Dennison, Experimentally derived resistivity for dielectric samples from the crres internal discharge monitor. *IEEE Trans. on Plasma Sci.* **2006,** *34*, (5), 1973-1978.

(80). Ng, N. L.; Kroll, J. H.; Chan, A.; Chhabra, P. S.; Flagan, R. C.; Seinfeld, J. H., Secondary organic aerosol formation from m-xylene, toluene, and benzene. *Atmos. Chem. Phys.* **2007,** *7*, (14), 3909-3922.

(81). Luo, H.; Chen, J.; Li, G.; An, T., Formation kinetics and mechanisms of ozone and secondary organic aerosols from photochemical oxidation of different aromatic hydrocarbons: dependence on NOx and organic substituents. *Atmos. Chem. Phys.* **2021,** *21*, (10), 7567-7578.

(82). Wolfe, G. M.; Marvin, M. R.; Roberts, S. J.; Travis, K. R.; Jin, L., The Framework for 0-D Atmospheric Modeling (F0AM) v3.1. *Geosci. Model Dev.* **2016,** *9*, (9), 3309-3319.

(83). Pinho, P. G.; Pio, C. A.; Carter, W. P. L.; Jenkin, M. E., Evaluation of alkene degradation in the detailed tropospheric chemistry mechanism, MCM v3, using environmental chamber data. *J. Atmos. Chem.* **2006,** *55*, (1), p.55-79.

(84). Chu, B.; Jiang, J.; Lu, Z.; Wang, K.; Li, J.; Hao, J., *Effects of Inorganic Seeds on Secondary Organic Aerosol*

(SOA) Formation. Atmospheric Aerosols - Regional Characteristics - Chemistry and Physics: 2012.
(85). Wang, W. G.; Li, K.; Zhou, L.; Ge, M. F.; Hou, S. Q.; Tong, S. R.; Mu, Y. J.; Jia, L., Evaluation and Application of Dual-Reactor Chamber for Studying Atmospheric Oxidation Processes and Mechanisms. *Acta Phys.-Chim. Sin.* **2012,** *31*, (7), 1251-1259.
(86).Bahreini, R.; Keywood, M.; Ng, N.; Varutbangkul, V.; Gao, S.; Flagan, R.; Seinfeld, J.; Worsnop, D.; Jimenez, J., Measurements of secondary organic aerosol from oxidation of cycloalkenes, terpenes, and m-xylene using an Aerodyne aerosol mass spectrometer. *Environ. Sci. Technol.* **2005,** *39*, (15), p. 5674-5688.
(87). Alfarra, M. R.; Paulsen, D.; Gysel, M.; Garforth, A.; Dommen, J.; PrévT, A.; Worsnop, D. R.; Baltensperger, U.; Coe, H., A mass spectrometric study of secondary organic aerosols formed from the photooxidation of anthropogenic and biogenic precursors in a reaction chamber. *Atmos. Chem. Phys.* **2006,** *6*, (12), 5279-5293.